1 **Delineating multiple salinization processes in a coastal plain aquifer, northern China:**
2 **hydrochemical and isotopic evidence**

4 Han Dongmei[a,b], Matthew Currell[c]
5 *a Key Laboratory of Water Cycle & Related Land Surface Processes, Institute of Geographic Sciences and Natural Resources*
6 *Research, Chinese Academy of Sciences, Beijing, 100101, China*
7 *b College of Resources and Environment, University of Chinese Academy of Sciences, Beijing 100049, China*
8 *c School of Engineering, RMIT University, Melbourne VIC 3000, Australia.*

10 **Abstract**

11 Groundwater is an important water resource for agricultural irrigation, urban and industrial utilization in the

12 coastal regions of northern China. In the past five decades, coastal groundwater salinization in the

13 Yang-Dai River plain has become increasingly serious under the influence of anthropogenic activities and

14 climatic change. It is pivotal for the scientific management of coastal water resources to accurately

15 understand groundwater salinization processes and their causative factors. Hydrochemical (major ion and

16 trace element) and stable isotopic ($\delta^{18}O$ and $\delta^2H$) analysis of different water bodies (surface water,

17 groundwater, geothermal water, and seawater) were conducted to improve understanding of groundwater

18 salinization processes in the plain's Quaternary aquifer. Saltwater intrusion due to intensive groundwater

19 pumping is a major process, either by vertical infiltration along riverbeds which convey saline surface

20 water inland, and/or direct subsurface lateral inflow. Trends in salinity with depth indicate that the former

21 may be more important than previously assumed. The proportion of seawater in groundwater is estimated

22 to have reached up to 13% in shallow groundwater of a local well field. End-member mixing calculations

23 also indicate that the geothermal water with high TDS (up to 10.6 g/L) with depleted stable isotope

24 compositions and elevated strontium concentrations (>10 mg/L) also locally mixes with water in the

25 overlying Quaternary aquifers. This is particularly evident in samples with elevated Sr/Cl ratios (>0.005

26 mass ratio). Deterioration of groundwater quality by salinization is also clearly exacerbated by

27 anthropogenic pollution. Nitrate contamination via intrusion of heavily polluted marine water is evident

28 locally (e.g. in the Zaoyuan well field); however, more widespread nitrate contamination due to other local

29 sources such as fertilizers and/or domestic wastewater is evident on the basis of $NO_3/Cl$ ratios. This study

30 provides an example of how multiple geochemical indicators can delineate different salinization processes

31 and guide future water management practices in a densely populated water-stressed coastal region.

32 **Key words:** Groundwater salinization; Stable isotopes; Coastal aquifers, Water quality

## 1. Introduction

Coastal regions are key areas for the world's social and economic development. Approximately 40% of the world's population lives within 100 kilometers of the coast (UN Atlas, 2010). Worldwide, these areas have become increasingly urbanized, with 14 of the world's 17 largest cities located along coasts (Creel, 2003). China has 18,000 km of continental coastline, and around 164 million people (approximately 12% of the total population) living in 14 coastal provinces; nearly 80% of these people inhabit three coastal 'economic zones', namely Beijing-Tianjin-Hebei, the Yangtze River delta and the Pearl River delta (Shi, 2012). The rapid economic development and growing population in these regions have greatly increased demand for fresh water. Meanwhile, they are also confronted with increased sewage and other wastewater discharge into coastal environments.

Groundwater resources play crucial roles in the social, economic and ecologic function of global coastal systems (IPCC, 2007). Coastal aquifers connect with the ocean and with continental hydro-ecological systems (Moore, 1996; Ferguson and Gleeson, 2012). As an important freshwater resource, groundwater may be over-extracted during periods of high demand, which are often periods of low recharge and/or surface water availability (Post, 2005). Over-exploitation of groundwater can therefore result in seawater intrusion, as well as related environmental issues such as land subsidence. Seawater intrusion has become a global issue and related studies can be found from coastal aquifers around the world, including Israel (Sivan et al., 2005; Yechieli et al., 2009; Mazi et al., 2014), Spain (Price and Herman, 1991; Pulido-Leboeuf, 2004; Garing et al., 2013), France (Barbecot et al., 2000; de Montety et al., 2008), Italy (Giambastiani et al., 2007; Ghiglieri et al., 2012), Morocco (Bouchaou et al., 2008; El Yaouti et al., 2009), USA (Gingerich and Voss, 2002; Masterson, 2004; Langevin et al., 2010), Australia (Zhang et al., 2004; Narayan et al., 2007; Werner, 2010), China (Xue et al., 2000; Han et al., 2011, 2015), Vietnam (An et al., 2014), Indonesia (Rahmawati et al., 2013), India (Radhakrishna, 2001; Bobba, 2002) and Brazil (Montenegro et al., 2006; Cary et al., 2015). Werner et al. (2013) provides a comprehensive review of seawater intrusion processes, investigation and management.

Seawater/saltwater intrusion is a complicated hydrogeological process, due to the impact of aquifer properties, anthropogenic activities (e.g., intensive groundwater pumping, irrigation practices), recharge rates, variable density flow, tidal activity and effects relating to global climate change, such as sea level rise (Ghassemi et al., 1993; Robinson et al., 1998; Smith and Turner, 2001; Simpson and Clement, 2004; Narayan et al., 2007; Werner and Simmons, 2009; Wang et al., 2015). Understanding the complex

63    interactions between groundwater, surface water, and seawater is thus essential for effective management of

64    coastal water resources (Mondal et al., 2010). Very different salinization patterns may arise as a result of

65    diverse interactions in coastal settings (Sherif and Singh, 1999; Bobba, 2002; Westbrook et al., 2005).

66    Modeling has shown that generally, seawater intrusion is more sensitive to groundwater pumping and

67    recharge rates in comparison to tidal fluctuation and sea level rise (Narayan et al., 2007; Ferguson and

68    Gleeson, 2012). However, most models of seawater intrusion require simplification of the coastal interface

69    zone. Relatively few studies have focused on delineating complex interactions among the

70    surface-ground-sea-water continuum in estuarine environments, including the effects of vertical infiltration

71    of seawater into aquifers through river channels, as compared to sub-surface lateral landward migration of

72    the freshwater-saltwater interface. Recent data indicate that such processes may be more important in

73    causing historical salinization of coastal groundwater than previously appreciated (e.g. Cary et al., 2015;

74    Lee et al., 2016; Larsen et al., 2017).

75    Additionally, groundwater in coastal aquifers may be affected by other salinization processes, such as

76    input of anthropogenic contaminants or induced mixing with saline water from deeper or adjacent

77    formations, which may include the high TDS-geothermal water or brines emplaced in the coastal zone over

78    geologic history. The data from China's marine environment bulletin released on March 2015 by the State

79    Oceanic Administration showed that the major bays, including Bohai Bay, Liaodong Bay and Hangzhou

80    Bay, are seriously polluted, with inorganic nitrogen and active phosphate being the major pollutants (SOA,

81    2015). Seawater intrusion in China is most serious in the Circum-Bohai-Sea region (Han et al., 2011,

82    2016a); and due to the heavy marine pollution, the impacts of anthropogenic activities on groundwater

83    quality in future may not simply be a case of simple salt-water intrusion. This region is also characterized

84    by deep brines and geothermal waters (e.g. Han et al., 2014), which may migrate and mix with fresher

85    groundwater under due to intensive water extraction. Depending on the specific processes involved,

86    additional contaminants may mix with fresh groundwater resources in parallel with seawater intrusion, and

87    it is thus likely to be more difficult to mitigate and remediate groundwater pollution.

88    A variety of approaches can be used to investigate and differentiate seawater intrusion and other

89    salinization processes, including time-series water level and salinity measurements, geophysical methods,

90    conceptual and mathematical modeling as well as geochemical methods (see reviews by Jones et al., 1999;

91    Werner et al., 2013). Geochemical techniques are particularly valuable in areas where the dynamics of

92    saline intrusion are complicated and may involve long-term processes pre-dating accurate water level

records, or where multiple salinization processes may be occurring simultaneously. These techniques typically employ the use of major ion ratios such as Cl/Br and Cl/Na, which are indicative of solute origins (Edmunds, 1996; Jones et al., 1999). Other ionic ratios, involving Mg, Ca, Na, HCO$_3$ and SO$_4$, and characterization of water 'types' can also be useful in determining the geochemical evolution of coastal groundwater, for example, indicating freshening or salinization, due to commonly associated ion exchange and redox reactions (Anderson et al., 2005; Walraevens, 2007). Trace elements such as strontium, lithium and boron can provide additional valuable information about sources of salinity and mixing between various end-members, as particular waters can have distinctive concentrations (and/or isotopic compositions) of these elements (e.g., Vengosh et al., 1999). Stable isotopes of water ($\delta^{18}$O and $\delta^2$H) are also commonly used in such studies, as they are sensitive indicators of water and salinity sources, allowing seawater to be distinguished from other salt sources (e.g., Currell et al., 2015).

This study examines the Yang-Dai River coastal plain in Qinhuangdao City, Hebei province, north China, specifically focusing on salinization of fresh groundwater caused by groundwater exploitation in the Zaoyuan well field and surrounding areas. The study investigates groundwater salinization processes and interactions among surface water, seawater and geothermal groundwater in a dynamic environment, with significant pressure on water resources. Qinhuangdao is an important port and tourist city of northern China. In the past 30 years, many studies have investigated seawater intrusion and its influencing factors in the region using hydrochemical analysis (Xu, 1986; Yang et al., 1994, 2008; Chen and Ma, 2002; Sun and Yang, 2007; Zhang, 2012) and numerical simulations (Han, 1990; Bao, 2005; Zuo, 2009). However, these studies have yet to provide clear resolution of the different mechanisms contributing to salinization, and have typically ignored the role of anthropogenic pollution and groundwater-surface water interaction. This study is thus a continuation of previous investigations of the region, using a range of hydrochemical and stable isotopic data to delineate the major processes responsible for increasing groundwater salinity, including lateral sub-surface sea-water intrusion, vertical leakage of marine-influenced surface water, induced mixing of saline geothermal water, and anthropogenic pollution. The goal is to obtain a more robust conceptual model of the interconnections between the various water sources under the impact of groundwater exploitation. The results provide significant new information to assist water resources management in the coastal plain of Bohai Bay, and other similar coastal areas globally.

## 2. Study area

The Yang-Dai River coastal plain (Fig. 1) covers approximately 200km$^2$ of the west side of Beidaihe District of Qinhuangdao City, northeastern Hebei Province. It is surrounded by the Yanshan Mountains to the north and west, and the southern boundary of the study area is the Bohai Sea. The plain declines in topographic elevation (with an average slope of 0.008) from approximately 390m above sea-level in the northwest to 1-25m in the southeast, forming a fan-shaped distribution of incised piedmont-alluvial plain sediments. Zaoyuan well field, located in the southern edge of the alluvial fan, approximately 4.3km from the Yang River estuary, was built in 1959 (Xu, 1986) as a major water supply for the region (Fig. 1).

### 2.1 Climate and hydrology

The study area is in a warm and semi-humid monsoon climate. On the basis of a 56-year record in Qinhuangdao, the mean annual rainfall is approximately 640 mm, the average annual temperature approximately 11$^o$C, and mean potential evaporation 1469 mm. 75% of the total annual rainfall falls in July-September (Zuo, 2006), during the East Asian Summer Monsoon. The average annual tide level is 0.86m (meters above Yellow Sea base level), while the high and low tides are approximately 2.48m and -1.43m.

The Yanghe River and Daihe River, originating from the Yanshan Mountains, are the major surface water bodies in the area, flowing southward into the Bohai Sea (Fig. 1). The Yang River is approximately 100 km long with a catchment area of 1029 km$^2$ and average annual runoff of $1.11 \times 10^8$ m$^3$/a (Han, 1988). Dai River has a length of 35 km and catchment area of 290 km$^2$, with annual runoff of $0.27 \times 10^8$ m$^3$/a. The rivers become full during intense rain events, and revert to minimal flow during the dry season – in part this is related to impoundment of flow in upstream reservoirs.

### 2.2 Geological and hydrogeological setting

Groundwater in the area includes water in Quaternary porous sediment as well as fractured bedrock in the northern platform area. Fractured rock groundwater volume mainly depends on the degree of weathering and the nature and regularity of fault zones (Fig. 1). The strata outcropping in the west, north and eastern edge of the plain include Archean, Proterozoic and Jurassic aged metamorphic and igneous rocks, which also underlie the Quaternary sediments of the plain (from which most samples in this study were collected). The basement faults under Quaternary cover are mainly NE-trending and NW-trending (Fig. 1); these structures control the development and thickness of the overlying sediments, as well as the

150    distribution of hot springs and geothermal anomalies. Fault zones are thought to be the main channel for

151    transport of thermal water from deeper to shallower depths.

152        The Quaternary sediments are widely distributed in the area, with the thickness ranging from

153    approximately 5-80 m (mostly 20-40 m), up to more than 100 m immediately adjacent to the coastline. The

154    bottom of the Holocene ($Q_4$) unit in most areas consists of clay, making the groundwater in the coastal zone

155    confined or semi-confined, although there are no regional, continuous aquitards between several layers of

156    aquifer-forming sediments (Fig. 1b). The aquifer is mainly composed of medium sand, coarse sand and

157    gravel layers with a water table depth of 1-4 m in the phreatic aquifer, and deeper semi-confined

158    groundwater (where present and hydraulically separated from the phreatic aquifer) hosted in similar

159    deposits with a potentiometric surface 1-5 m below topographic elevation (Zuo, 2006).

160        The general flow direction of groundwater is from northwest to south, according to the topography.

161    The main sources of recharge are from infiltration of rainfall, river water and irrigation return-flow, as well

162    as lateral subsurface inflow from the piedmont area. Naturally, groundwater discharges into the rivers and

163    the Bohai Sea. Apart from phreatic water evaporation, groundwater pumping for agricultural, industrial and

164    domestic usage (including seasonal tourism) are currently the main pathways of groundwater discharge.

165        Geothermal water discharges into shallow Quaternary sediments near the fault zones, evident as

166    geothermal anomalies (Hui, 2009). The temperature of thermal water ranges from 27-57°C in this

167    low-to-medium temperature geothermal field (Zeng, 1991). Deeper thermal water is stored in the

168    Archaeozoic granite and metamorphic rocks; major fracture zones provide pathways into the overlying

169    Quaternary sediments (Pan, 1990; Shen et al., 1993; Yang, 2011).

170    **2.3 Groundwater usage and seawater intrusion history**

171        Shallow groundwater pumped from the Quaternary aquifer occupies 94% of total groundwater

172    exploitation, and is used for agricultural irrigation (52% of total groundwater use), industrial (32%) and

173    domestic water (16%) (Meng, 2004). Many large and medium-sized reservoirs were built in the 1960s and

174    1970s meaning that the surface water was intercepted and downstream runoff dropped sharply, even

175    causing rivers to dry up in drought years. With the intensification of human socio-economic activities and

176    growing urbanization, coupled with extended drought years (severe drought during 1976-1989 in north

177    China) (Wilhite,1993; Han et al., 2015), increased groundwater exploitation to meet the ever-growing fresh

178    water demand resulted in groundwater table declines and seawater intrusion (SWI) in the aquifers.

179       The pumping rate in the Zaoyuan well field gradually increased from 1.25 million $m^3$/a in the early

180     1960s to 3.5 million $m^3$/a in the late 1970s, and beyond 10 million $m^3$/a in the 1980s. During 1966-1989,

181     planting of paddy fields became common, resulting in significant agricultural water consumption. This

182     caused formation of a cone of depression in the Quaternary aquifer system. Groundwater pumping in this

183     region mainly occurs in spring and early summer, with typical pumping rates of 7~80,000 $m^3$/d. Pumping

184     from the Zaoyuan well-field occurs in wells approximately 15 to 20m deep. Groundwater tables decline

185     sharply and reach their lowest level during May, before the summer rains begin, and recover to their yearly

186     high in January-February (Fig. 2). In May 1986, the groundwater table in the depression center, which is

187     located in Zaoyuan-Jiangying (Figure S1), decreased to -2 m.a.s.l.(meters above sea level) and the area

188     with groundwater tables below sea level covered 28.2 $km^2$. The local government commenced reduction in

189     groundwater exploitation in this area after 1992, and groundwater tables began to decrease more slowly

190     after 1995, even showing recovery in some wells. However, during an extreme drought year (1999),

191     increased water demand resulted in renewed groundwater table declines in the region (Fig. 2). Since 2000,

192     the groundwater tables have responded seasonally to water demand peaks and recharge (Fig. 2; Fig. S1).

193       From 1990, the rapid development of township enterprises (mainly paper mills), also began to cause

194     groundwater over-exploitation in the western area of the plain. The groundwater pumping rate for paper

195     mills reached 55,000 $m^3$/d in 2002, resulting in groundwater table depressions around Liushouying and

196     Fangezhuang (Fig. 1). The groundwater table in the western depression associated with this pumping

197     reached -11.6 m.a.s.l. in 1991 and -17.4 in 2002. After the implementation of "Transfering Qing River

198     water to Qinhuangdao" project in 1992, the intensity of groundwater pumping generally reduced, and the

199     groundwater table in the depression center recovered to -4.3 m.a.s.l. in July 2006.

200       Overall, the depression area (groundwater tables below mean sea level) was recorded as 132.3$km^2$ in

201     May 2004 and the shape of the depression has generally been elliptical with the major axis aligned E-W. In

202     addition to groundwater over-exploitation, climate change-induced recharge reduction has also likely

203     contributed to groundwater table declines and hence seawater intrusion (Fig. S2). The annual average

204     rainfall declined from 639.7 mm between 1954 - 1979 to 594.2 mm between 1980 and 2010; a significant

205     decrease over the last 30 years (Zhang, 2012). As indicated in Figure S2, the severity of seawater intrusion

206     (indicated by changes in Cl concentration, and the total area impacted by SWI, as defined by the 250mg/L

207     Cl contour) correlates with periods of below average rainfall – indicated by monthly cumulative rainfall

208     departure (CRD, Weber and Stewart, 2004).

209       Groundwater quality of the area gradually became more saline from the early 1980s, with chloride

210     concentrations increasing year by year. As early as 1979, seawater intrusion was recorded in the Zaoyuan

211     well field. The intrusion area with groundwater chloride concentration greater than 250 mg/L was 21.8 km$^2$

212     in 1984, 32.4 km$^2$ in 1991, 52.6 km$^2$ in 2004 and 57.3 km$^2$ in 2007 (Zuo, 2006; Zang et al., 2010). The

213     chloride concentration of groundwater pumped from the a monitored well-field well (depth of 18 m, G10 in

214     Fig. 1) changed from 90 mg/L in 1963 to 218 mg/L in 1978, 567 mg/L in 1986, 459 mg/L in 1995, and

215     1367 mg/L in 2002 (Zuo, 2006), reducing to 812 mg/L in July 2007. The distance of estimated seawater

216     intrusion into the inland area from the coastline had reached 6.5 km in 1991, and 8.75 km in 2008 (Zang et

217     al., 2010). In the early 1990s, 16 of 21 pumping wells in the well field were abandoned due to the saline

218     water quality (Liang et al., 2010). Additionally, 370 of 520 pumping wells were abandoned in the wider

219     Yang-Dai River coastal plain during 1982-1991 (Zuo, 2006).

220   **3. Methods**

221       In total, 80 water samples were collected from the Yang-Dai River coastal plain, including 58

222     groundwater samples, 19 river water samples (from 12 sites) and 3 seawater samples, during three sampling

223     campaigns (June 2008, September 2009 and August 2010). Groundwater samples were pumped from 28

224     production wells with depths between 6 and 110m, including 7 deep wells with depths greater than 60m

225     (Fig. 1). While ideally, sampling for geochemical parameters would be conducted on monitoring wells, due

226     to an absence of these, production wells were utilised. In most cases, the screened interval of these wells

227     encompasses aquifer thicknesses of approximately 5 to 15m above the depths indicated in Table 1.

228       In this study, sampling focused predominantly on low temperature groundwater; however, geothermal

229     water from around Danihe was also considered a potentially important ongoing source of groundwater

230     salinity. As such, while geothermal water samples were not accessible during our sampling campaigns (as

231     the area is now protected), data reported by Zeng (1991) were compiled and analyzed in conjunction with

232     the sampled wells.

233       Measurements of physico-chemical parameters (pH, temperature, and electrical conductivity (EC))

234     were conducted in situ using a portable meter (WTW Multi 3500i). All water samples were filtered with

235     0.45 μm membrane filters before analysis of hydrochemical composition. Two aliquots in polyethylene

236     100mL bottles at each site were collected for major cation and anion analysis, respectively. Samples for

237     cation analysis ($Na^+$, $K^+$, $Mg^{2+}$ and $Ca^{2+}$) were treated with 6N $HNO_3$ to prevent precipitation. Water

238    samples were sealed and stored at 4°C until analysis. Bicarbonate was determined by titration within 12

239    hours of sampling. Concentrations of cations and some trace elements (B, Sr, Li) were analyzed by

240    inductively coupled plasma-optical emission spectrometry (ICP-OES) in the chemical laboratory of the

241    Institute of Geographic Sciences and Natural Resources Research (IGSNRR), Chinese Academy Sciences

242    (CAS). Only the Sr data are reported here, as the other trace elements were not relevant to the

243    interpretations discussed (Table 1). The detection limits for analysis of $Na^+$, $K^+$, $Mg^{2+}$ and $Ca^{2+}$ are 0.03,

244    0.05, 0.009, and 0.02 mg/L. Concentrations of major anions (i.e. $Cl^-$, $SO_4^{2-}$, $NO_3^-$ and $F^-$) were analyzed

245    using a High Performance Ion Chromatograph (SHIMADZU, LC-10ADvp) at the IGSNRR, CAS. The

246    detection limits for analysis of $Cl^-$, $SO_4^{2-}$, $NO_3^-$ and $F^-$ are 0.007, 0.018, 0.016, and 0.006 mg/L. The testing

247    precision the cation and anion analysis is 0.1-5.0%. Charge balance errors were less than 8%. Stable

248    isotopes ($\delta^{18}O$ and $\delta^2H$) of water samples were measured using a Finnigan MAT 253 mass spectrometer

249    after on-line pyrolysis with a Thermo Finnigan TC/EA in the Stable Isotope Laboratory of the IGSNRR,

250    CAS. The results are expressed in ‰ relative to international standards (V-SMOW (Vienna Standard Mean

251    Ocean Water)) and resulting $\delta^{18}O$ and $\delta^2H$ values are shown in Table 1. The analytical precision for $\delta^2H$ is

252    ±2‰ and for $\delta^{18}O$ is ±0.5‰. All hydrochemical, physico-chemical and isotope data are reported in Table 1.

253        Mixing calculations were also conducted on the basis of $Cl^-$ concentrations of the samples under a

254    conservative freshwater-seawater mixing system (Fidelibus et al., 1993; Appelo, 1994). The seawater

255    contribution for each sample is expressed as a fraction of seawater ($f_{sw}$), using (Appelo and Postma, 2005):

256
$$f_{sw} = \frac{C_{Cl,sam} - C_{Cl,f}}{C_{Cl,sw} - C_{Cl,f}} \tag{1}$$

257        where $C_{Cl,sam}$, $C_{Cl,f}$, and $C_{Cl,sw}$ refer to the $Cl^-$ concentration in the sample, freshwater, and seawater,

258    respectively.

259

## 4. Results

261    4.1 Water stable isotopes ($\delta^2H$ and $\delta^{18}O$)

262        The local meteoric water line (LMWL, $\delta^2H=6.6\ \delta^{18}O+0.3$, n=64, $r^2=0.88$) is based on $\delta^2H$ and $\delta^{18}O$

263    mean monthly rainfall values between 1985 and 2003 from Tianjin station some 120 km SW of

264    Qinhuangdao City (IAEA/WMO, 2006). Due to similar climate and position relative to the coast, this can

265    be regarded as representative of the study area. Surface water samples collected from Yang River and Dai

266    River (n = 19) have $\delta^{18}O$ and $\delta^2H$ values ranging from -10.1 to -0.6‰ (mean= -5.4‰) and -71 to-11‰

267 (mean = -43‰), respectively. Stable isotope compositions for surface water appear to exhibit significant

268 seasonal variation (Fig. S3); for Yang River samples from the relatively dry season (June 2008, n = 3) had

269 mean $\delta^{18}O$ and $\delta^2H$ values of -3.0‰ -31‰, respectively; samples from the wet season (August 2009 and

270 September 2010, n = 6) had mean $\delta^{18}O$ and $\delta^2H$ values of -6.6‰ -48‰, respectively. Dai River samples

271 showed similar results; the dry season mean $\delta^{18}O$ and $\delta^2H$ values (n = 3) were -2.6‰ and -32‰,

272 respectively; wet season samples (n = 7), had mean $\delta^{18}O$ and $\delta^2H$ values of -6.6‰ and -49‰, respectively

273 (Fig. 3).

274       The 56 groundwater samples were characterized by $\delta^{18}O$ and $\delta^2H$ values ranging from -11.0 to -4.2‰

275 (mean= -6.5‰) and -76 to -39‰ (mean = -50‰), respectively. Among these, shallow and deep

276 groundwater samples showed similar mean values, although deep groundwater samples (n = 13) showed

277 relatively narrow overall ranges (-7.8 to -5.1‰ and mean = -6.3‰ for $\delta^{18}O$; -58 to -43‰ and mean = -50‰

278 for $\delta^2H$; Fig. 3). Slight seasonal variation was evident in the groundwater isotope compositions; shallow

279 groundwater from the dry season (n = 12) showed $\delta^{18}O$ and $\delta^2H$ values from -7.2 to -4.2‰ (mean = -5.7‰)

280 and $\delta^2H$ values from -56 to -39‰ (mean = -48‰); while during the wet season (n = 31) $\delta^{18}O$ and $\delta^2H$

281 values ranged from -11.0 ~ -5.3‰ (mean = -6.9‰) and -76 ~ -43‰ (mean = -51‰), respectively. Some

282 variability was also evident in deep groundwater compositions, although only three deep samples were

283 collected during the dry season.

284       From Figure 3, it can be seen that surface water exhibits a much wider range of $\delta^{18}O$ and $\delta^2H$ values

285 relative to groundwater, with shallow groundwater in turn more spatially variable than deep groundwater.

286 Water samples collected in the wet season showed wider ranges of $\delta^{18}O$ and $\delta^2H$ values relative to the dry

287 season. Most water samples of all types plot to the right of (below) the LMWL, with some surface water

288 samples showing similar compositions to the local seawater (Fig. 3). The local seawater plots below (more

289 negative) than typically assumed values (e.g. VSMOW = 0‰) for both $\delta^2H$ and $\delta^{18}O$, and this water

290 appears to represent an end-member involved in mixing with meteoric-derived waters in both ground and

291 surface water (Fig. 3).

292 4.2 Water salinity and dissolved ions

293       TDS (total dissolved solids) concentrations of surface water samples from Dai River range from

294 0.3g/L~31.4g/L with $Na^+$ and $Ca^{2+}$ comprising 22-78% and 4-56% of total cations and $Cl^-$ comprising

295 36-91% of total anions. The composition changes from Ca•Na•Mg-Cl•HCO$_3$ to Na-Cl water type from

upstream to downstream locations along with increasing salinity; $Cl^-$ concentrations vary from approximately 70 mg/L upstream to 16700 mg/L near the coastline, due to marine influence. Similar variation occurs along the Yang River, where samples had TDS concentrations between 0.3-26.1 g/L with increasing concentrations and proportions of $Cl^-$ (63.2-14953.5 mg/L) from upstream to downstream locations. Nitrate concentrations also range from 2.8 to 65.2 mg/L in the surface water samples, increasing downstream.

In the early 1960s, groundwater pumped from the Zaoyuan well field exhibited $Ca-HCO_3$ water type and chloride concentrations of 90-130 mg/L; this was followed by rapid salinization since the 1980s (see section 2.3). In this study, shallow groundwater is characterized by TDS concentrations of 0.4-4.8 g/L with $Cl^-$ (34-77%), $Na^+$ (12-85%) and $Ca^{2+}$ (5-69%) being the predominant major anion and cations, respectively. Groundwater hydrochemical types vary from $Ca-HCO_3•Cl$, $Ca•Na-Cl$, $Na•Ca-Cl$ to $Na-Cl$ (Figure 4). Deep groundwater has TDS concentrations between 0.3-2.8g/L, dominated by Ca (up to 77% of major cations) in the upstream area and Na (up to 85% or major cations) near the coast, with water type evolving from $Ca-Cl•HCO_3$ to $Ca•Na-Cl$ and $Na•Mg-Cl$ (Figure 4). At present, the TDS of groundwater from the well field reaches 3.31 g/L with $Na-Cl$ water type (see well G15). The highest observed mixing proportions of seawater occur in shallow well G10 and deep well G2, respectively, with calculated *fsw* values (according to equation 1) of 12.95% and 5.35%, respectively.

Hydrochemical features of thermal water from the Danihe-Luwangzhuang area (Fig. 1A) are distinct from the normal/low temperature groundwater. Previous work by Zeng (1991) and Hui (2009) identified geothermal water with high TDS in the fractures of deep metamorphic rock. The geothermal water was characterized by TDS values between 6.2-10.6 g/L and $Ca•Na-Cl$ water type, while $Cl^-$ concentrations ranged from 5.4 to 6.5 g/L and Sr concentrations from 6.73 to 89.8 mg/L. Some normal/low temperature groundwater samples collected in this study from wells G8, G19, and G9 featured by $Ca•Na-Cl$ water type with relative high TDS ranges (0.8-1.4 g/L, 1.3-1.6 g/L, and1.5-2.8 g/L, respectively) and strontium concentrations (1.1-1.9 mg/L, 4.9-7.1 mg/L, and 7.3-11.6 mg/L, respectively), showing similarity with the geothermal system. Low temperature groundwater sampled in this study had Sr/Cl mass ratios ranging from $2.4 \times 10^{-4}$ to $1.6 \times 10^{-2}$, with higher ratios in deep groundwater (range: $9.4 \times 10^{-4}$ to $1.3 \times 10^{-2}$, median: $3.7 \times 10^{-3}$) compared to shallow groundwater (median: $3.1 \times 10^{-3}$), and groundwater generally higher than seawater/saline surface water (range: $3.7 \times 10^{-4}$ to $5.8 \times 10^{-4}$, median: $3.9 \times 10^{-4}$; Table S1).

Nitrate concentrations in groundwater range from 2.0-178.5 mg/L (mean 90.1 mg/L) for shallow

326    groundwater, and 2.0-952.1 mg/L (mean 232.1 mg/L) for the deep groundwater, respectively, with most

327    samples exceeding the WHO drinking water standard (50 mg/L).

## 5. Discussion

5.1 Groundwater isotopes and hydrochemistry as indicators of mixing processes

330    The Quaternary groundwater system in the Yang-Dai River coastal plain may be recharged by

331    precipitation, irrigation return flow, river infiltration and lateral subsurface runoff (e.g. from mountain-front

332    regions). Groundwater geochemical characteristics are then controlled by hydrogeological conditions and

333    mixing processes, including mixing induced by extensive groundwater pumping, as well as natural mixing

334    and water-rock interaction. It is evident from the geochemistry that mixing has occurred between

335    groundwater and seawater in the coastal areas, as well as between normal/low temperature groundwater and

336    geothermal water in the inland areas (e.g. near the Danihe geothermal field). Different sources of water are

337    generally characterized by somewhat distinctive stable isotopic and hydrochemical compositions, allowing

338    mixing calculations to aid understanding of the groundwater salinization and mixing processes, as

339    discussed below.

340    Stable isotopes of O and H in groundwater and surface water fall on a best-fit regression line (dashed

341    line in Fig. 3) with slope of $\delta^2H=4.4\times\delta^{18}O-21.7$, significantly lower than either the local or global meteoric

342    water lines. Three processes are likely responsible for the measured range of isotopic compositions: 1.

343    Mixing between saline surface water (e.g. seawater or saline river water affected by tidal ingress) and

344    fresher, meteoric-derived groundwater or surface water; 2. Mixing between fresh meteoric-derived

345    groundwater and saline thermal water; 3. Evaporative enrichment of surface water and/or irrigation

346    return-flow, which may infiltrate groundwater in some areas. A sub-group of surface water samples (e.g.,

347    S1 to S3, S7 and S12; termed 'brackish surface water') show marine-like stable isotopic compositions and

348    major ion compositions (Fig. 3 and Fig. 5). The 'fresh' surface water samples (e.g. EC values <1500 μS/cm)

349    exhibit meteoric-like stable isotope compositions, with some samples (such as S9 and S10) showing clear

350    evidence of evaporative enrichment in the form of higher $\delta^2H$ and particularly, $\delta^{18}O$ values (Fig. 3).

351    Fresh groundwater has depleted $\delta^{18}O$ and $\delta^2H$ values relative to seawater and show a clear meteoric

352    origin, albeit with modification due to mixing. Theoretically, the mixing of meteoric-derived fresh

353    groundwater and marine water should result in a straight mixing line connecting the two end members;

354    however this is also complicated in the study area by the possible mixing with geothermal water. The

355 thermal groundwater has distinctive stable isotopic and major ion composition (Han, 1988; Zeng, 1991),

356 allowing these mixing processes to be partly delineated. Stable isotopes of thermal groundwater are more

357 depleted than low-temperature groundwater (e.g. $\delta^{18}O$ values of approximately -8‰, Fig. 8), indicating this

358 likely originates from the mountainous areas to the north; Zeng (1991) estimated the elevation of the

359 recharge area for the geothermal field to be from 1200 to 1500 m.a.s.l. Based on a bivariate plot of $\delta^{18}O$ vs.

360 Cl⁻ with mixing lines and defined fresh and saline end-members, Fig. 5 shows the estimated degree of

361 mixing between fresh groundwater including shallow (G4) and deep (G25) groundwater end-members, and

362 saline water, including seawater and geothermal end-members.

363     The two fresh end-members were selected to represent a range of different groundwater

364 compositions/recharge sources, from shallow water that is impacted by infiltration of partially evaporated

365 recharge (fresh but with enriched $\delta^{18}O$) to deeper groundwater unaffected by such enrichment (fresh and

366 with relatively depleted $\delta^{18}O$). The narrower range and relatively enriched stable isotopes in shallow

367 groundwater samples collected during the dry season compared with the wet season indicate some

368 influence of seasonal recharge by either rainfall (fresh, with relatively depleted stable isotopes) or irrigation

369 water subject to evaporative enrichment (more saline, with enriched stable isotopes and high nitrate

370 concentrations; Currell et al., 2010) and/or surface water leakage. While there is overlap in the isotopic and

371 hydrochemical compositions of shallow and deep groundwater (Fig. 3 & Fig. 4), this effect appears to only

372 affect the shallow aquifer.

373     Based on Fig. 5, the shallow groundwater samples (e.g. G15, G10, G11, G14) collected from or

374 around the Zaoyuan well field appear to be characterized by mixing between fresh meteoric water and

375 seawater (plotting in the upper part of Fig. 5); while some deeper groundwater samples (e.g. G13, G2, G16,

376 G14) collected from the coastal zone also appearing to indicate mixing with seawater. Groundwater

377 sampled relatively close to the geothermal field (e.g. G9, G19) shows compositions consistent with mixing

378 between low-temperature fresh water and saline thermal water (lower part of Fig. 5). This is more evident

379 in deep groundwater than shallow groundwater, which is consistent with mixing from below, as expected

380 for the deep-source geothermal water. Other samples impacted by salinization show more ambiguous

381 compositions between the various mixing lines, which may arise due to mixing with either seawater,

382 geothermal water or a combination of both (e.g., G29).

383     The estimated mixing fraction ($f_{sw}$) of marine water for the shallow brackish groundwater ranges from

384 1.2~13.0% and 2.6~6.0% for the deep brackish groundwater. The highest fraction of 13% was recorded in

385 G10, located in the northerm part of the Zaoyuan well field, which is located near a tidally-impacted

386 tributary of the Yang River (Fig 1). Relatively higher fractions of marine water in relatively shallow

387 samples (including those from the well field) compared to deeper samples may indicate a more 'top down'

388 salinization process, related to leakage of saline surface water through the riverbed, rather than 'classic'

389 lateral sea water intrusion, which typically causes salinization at deeper levels due to migration of a salt

390 water 'wedge' (e.g. Werner et al., 2013); this is consistent with results of resistivity surveys conducted in

391 the region (Fig. 6). The profile of chloride concentrations vs. depth indicates that salinization affects

392 shallow and deep samples alike, with the most saline samples being relatively shallow wells in the Zaoyuan

393 well-field (Fig. 7).

394 In general, brackish and fresh groundwater samples show distinctive major ion compositions, with the

395 more saline water typically showing higher proportions of Na and Cl (Fig. 4). This contrasts with historic

396 data collected from the Zaoyuan well field, which showed Ca-$HCO_3$ type water with Cl concentrations

397 ranging from 130 to 170 mg/L. This provides additional evidence that the salinization in this area is largely

398 due to marine water mixing. More Ca-dominated compositions are evident in the region near the

399 geothermal well field further in-land (e.g., G5, G8, G19, G29, and G24); consistent with a component of

400 salinization that is unrelated to marine water intrusion. Plots of ionic ratios of Na/Cl and Mg/Ca vs. Cl also

401 reveal a sub-set of relatively saline deep groundwater samples which appear to evolve towards the

402 geothermal-type signatures with increasing salinity (Fig. 8).

403 Stronger evidence of mixing of the geothermal water in the Quaternary aquifers (particularly deep

404 groundwater) is provided by examining strontium concentrations in conjunction with chloride (Fig. 9). The

405 geothermal water from Danihe geothermal field has much higher Sr concentrations (up to 89.8 mg/L) than

406 seawater (5.4-6.5 mg/L in this study), due to Sr-bearing minerals (i.e., celestite, strontianite) with Sr

407 contents of 300-2000 mg/kg present in the bedrock (Hebei Geology Survey, 1987). Groundwater sampled

408 from near the geothermal field in this study has the highest Sr concentrations e.g., G9 with Sr

409 concentrations ranging from 7.4 to 11.6 mg/L, and G19 from 4.9 to 7.1 mg/L.

410 The plot of chloride versus strontium concentrations (Fig. 9) shows that these samples and others (e.g.,

411 G16, G20, G27, G29) plot close to a mixing line between fresh low-temperature and saline

412 thermal-groundwater. Mass ratios of Sr/Cl in these samples are also elevated relative to seawater by an

413 order of magnitude or more (e.g. Sr/Cl >$5.0 \times 10^{-3}$, compared to $3.9 \times 10^{-4}$ in seawater, Table S1). Other

414 samples from closer to the coast (e.g. G4) also approach the thermal-low temperature mixing line,

415    indicating probable input of thermal water. Samples collected from the Zaoyuan well field generally plot

416    closer to the Sr/Cl seawater mixing line (consistent with salinization largely due to marine water – Fig. 9);

417    however, samples mostly plot slightly above the mixing line with additional Sr, which may indicate more

418    widespread (but volumetrically minor) mixing with the thermal water in addition to seawater.

419    5.2 Anthropogenic pollution of groundwater

420        The occurrence of high nitrate (and possibly also sulfate) concentrations in groundwater in both

421    coastal and in-land areas also indicates that anthropogenic pollution is an important process impacting

422    groundwater quality and salinity (Fig. 10; Table 1). Seawater from Bohai Sea is heavily affected by nutrient

423    contamination, showing $NO_3^-$ concentrations of 810 mg/L in this study, and up to 1092 mg/L in seawater

424    further north of the bay near Dalian (Han et al., 2015), primarily due to wastewater discharge into the sea.

425    The historic sampled $NO_3^-$ concentration of groundwater in the well field increased from 5.4 mg/L in May

426    1985 to 146.8~339.4 mg/L in Aug 2010, while the concentration in seawater changed from 57.4 mg/L in

427    May1985 to 810.1 mg/L in Aug 2010. A bivariate plot of Cl- vs. $NO_3^-$ concentrations in groundwater (Fig.

428    10) can thus be used to identify nitrate sources and mixing trends, including infiltration with contaminated

429    seawater, and other on-land anthropogenic $NO_3$-sources (e.g. domestic/industrial wastewater discharge

430    and/or $NO_3^-$-bearing fertilizer input through irrigation return-flow).

431        From this plot (Fig. 10) it appears that the major source of $NO_3^-$ in groundwater is on-land

432    anthropogenic inputs rather than mixing with seawater, which would result in relatively large increases in

433    Cl along with $NO_3$. Samples G10 and G15 (from the well field) are exceptions to this trend, showing clear

434    mixing with nitrate-contaminated seawater. Deep groundwater (e.g. G9, G14) is also extensively

435    contaminated with high $NO_3^-$ concentrations; this is likely associated with leakage from the surface via

436    poorly constructed or abandoned wells - a problem of growing significance in China (see Han et al., 2016b;

437    Currell and Han, 2017). According to one investigation by Zang et al.(2010), 14 of 21 pumping wells in the

438    Zaoyuan well field have been abandoned due to poor water quality, and 307 pumping irrigation wells

439    (occupied 2/3 of total pumping wells for irrigation) in the region have also been abandoned. Local

440    authorities have however not implemented measures to deal with abandoned wells, meaning they are a

441    future legacy contamination risk – e.g. by allowing surface runoff impacted by nitrate contamination to

442    infiltrate down well annuli.

## 5.3 Hydrochemical evolution during salinization

A hydrogeochemical facies evolution diagram (HFE-D) proposed by Giménez-Forcada (2010), was used to analyze the geochemical evolution of groundwater during seawater intrusion and/or freshening phases (Fig. 11). In the coastal zone, the river water shows an obvious mixing trend between fresh and saline end members. Some shallow groundwaters (e.g., G2, G4, G10, G13, G15) are also close to the mixing line between the surface-water end-members on this figure, indicating mixing with seawater without significant additional modification by typical water-rock interaction processes (e.g. ion exchange). Most brackish groundwaters (e.g., G11, G16, G17, G20, G25, G28, G29) have evolved in the series $Ca-HCO_3 \rightarrow Ca-Cl \rightarrow Na-Cl$, according to classic seawater intrusion. A relative depletion in Na (shown in lower than marine Na/Cl ratios) and enrichment in Ca (shown as enriched Ca/SO$_4$ ratios) is evident in groundwater with intermediate salinities (e.g. Fig. 8; Fig. 11), indicating classic base-exchange between Na and Ca during salinization (Appelo and Postma, 2005). Locally, certain brackish water samples (e.g., G1, G12, G26) appear to plot in the 'freshening' part of the HFE diagram (potentially indicating slowing or reversal of salinisation due to reduce in groundwater use), although these do not follow a conclusive trajectory. Water samples from the geothermal field (G5, G8, G9, and G19) plot in a particular corner of the HFE diagram away from other samples (being particularly Ca-rich); a result of their distinctive geochemical evolution during deep transport through the basement rocks at high temperatures.

## 5.4 Conceptual model of salinization and management implications

Coastal zones encompass the complex interaction among different water bodies (i.e., river water, seawater and groundwater). The interactions between surface- and ground-water in the Yang-Dai River coastal plain have generally been ignored in previous studies. However, the surface water chemistry data show that the distribution of salt water has historically reached more than 10 km inland along the estuary of the Yang River, and approximately 4 km inland in the Dai River (Han, 1988). The relatively higher proportion of seawater-intrusion derived salinity in shallow samples in this study, along with the evidence from resistivity surveys (Fig. 6; Zuo, 2006) indicate that intrusion by vertical leakage from these estuaries is therefore an important process. The hazard associated with this pathway in recent times has been reduced by the construction of a tidal dam, which now restricts seawater ingress along the Yang estuary to within 4 km of the coastline. This may alleviate salinization to an extent in future in the shallow aquifer by removing one of the salinization pathways, however, as described, there are multiple other salinization

472    processes impacting the groundwater in the Quaternary aquifers of the region.

473        A conceptual model of the groundwater flow system in the Yang-Dai River coastal plain is

474    summarized in Fig. 12. This model presents an advance on the previous understanding of the study area, by

475    delineating four major processes responsible for groundwater salinization in this area. These are: 1.

476    Seawater intrusion by lateral sub-surface flow; 2. Interaction between saline surface water and groundwater

477    (e.g. vertical leakage of saline water from the river estuaries); 3. Mixing between low-temperature

478    groundwater and deep geothermal water; and, 4. Irrigation return-flow and associated anthropogenic

479    contamination. Both the lateral and vertical intrusion of saline water are driven by the long-term

480    over-pumping of groundwater from fresh aquifers in the region. The irrigation return-flow from local

481    agriculture results from over-irrigation of crops, and is responsible for extensive nitrate pollution (up to 340

482    mg/L $NO_3^-$ in groundwater of this area) probably due to dissolution of fertilizers during infiltration. The

483    somewhat enriched stable isotopes in shallow groundwater (more pronounced in the dry season) also

484    indicate that such return-flow may recharge water impacted by evaporative salinization into the aquifer.

485    The geothermal water, with distinctive chemical composition (e.g. depleted stable isotopes, high TDS, Ca

486    and Sr concentrations), is also demonstrated in this study to be a significant contributor to groundwater

487    salinization, via upward mixing. The study area is therefore in a situation of unusual vulnerability, in the

488    sense that it faces salinization threats simultaneously from lateral, downward and upward migration of

489    saline water bodies.

490        According to drinking water standards and guidelines from China Environmental Protection Authority

491    (GB 5749-2006) and/or US EPA and WHO, chloride concentration in drinking water should not exceed 250

492    mg/L. At the salinity levels observed in this study - many samples impacted by salinization

493    contain >500mg/L of chloride (Table 1) - a large amount of groundwater is now or will soon be unsuitable

494    for domestic usage, as well as irrigation or industrial utilization. So far, this has enhanced the scarcity of

495    fresh water resources in this region, leading to a cycle of groundwater table decline → seawater intrusion

496    → loss of available freshwater → increased pumping of remaining fresh water. If this cycle continues, it is

497    likely to further degrade groundwater quality and restrict its usage in the future. Such a situation is typical

498    of the coastal water resources 'squeeze' highlighted by Michael et al., (2017). Alternative management

499    strategies, such as restricting water usage in particular high-use sectors, such as agriculture, industry or

500    tourism, that are based on a comprehensive assessment of the social, economic and environmental benefits

501    and costs of these activities, warrants urgent and careful consideration.

## 6. Conclusions

Groundwater in the Quaternary aquifers of the Yang-Dai River coastal plain is an important water resource for agricultural irrigation, domestic use (including for tourism) and industrial activity. Extensive groundwater utilization has made the problem of groundwater salinization in this area increasingly prominent, resulting in the closure of wells in the area. Based on the analysis of hydrochemical and stable isotopic compositions of different water bodies, we delineated the key groundwater salinization processes. Seawater intrusion is the main process responsible for salinization in the coastal zone; however this likely includes vertical saltwater infiltration along the riverbed into aquifers as well as lateral seawater intrusion caused by pumping for fresh groundwater at the Zaoyuan wellfield. The upward mixing of high TDS-geothermal water into the Quaternary aquifers is also evident, particularly through the use of stable isotope, chloride and strontium end-member mixing analysis. Additionally, significant nitrate pollution from the anthropogenic activities (e.g., agricultural irrigation return-flow with dissolution of fertilizers) and locally, intrusion of heavily polluted seawater, are also evident.

Groundwater salinization has become a prominent water environment problem in the coastal areas of northern China (Han et al., 2014; Han et al., 2015; Han et al., 2016a), and threatens to create further paucity of fresh water resources, which may prove a significant impediment to further social and economic development in these regions. Since the 1990s, the local government has begun to pay attention to the problem of seawater intrusion, and irrational exploitation of groundwater has been restricted in some cases. The Zaoyuan well field ceased to pump groundwater since 2007, while an anti-tide dam (designed to protect against tidal surge events) established in the Yang River estuary may also reduce saline intrusion in future. However, due to the significant lag-time associated with groundwater systems, a response in terms of water quality may take time to emerge, and in the meantime the other salinization and pollution impacts documented here may continue to threaten water quality. In this regard, we recommend continued monitoring of groundwater quality and levels, and active programs to reduce input of anthropogenic contaminants such as nitrate from fertilizers, and appropriate well-construction and decommissioning protocols to prevent contamination through preferential pathways.

## Acknowledgement

This research was supported by Zhu Kezhen Outstanding Young Scholars Program in the Institute of Geographic Sciences and Natural Resources Research, Chinese Academy of Sciences (CAS) (grant number 2015RC102), and Outstanding member program of the Youth Innovation Promotion Association, CAS (grant number 2012040). The authors appreciate the helpful field work and data collection made by Mr

533 Yang Jilong from Tianjin Institute of Geology and Mineral Resources, Dr. Wang Peng and Dr Liu Xin from
534 Chinese Academy of Sciences.
535

## References

537 An T.D., Tsujimura M., Phu V.L., Kawachi A., Ha D.T., 2014. Chemical Characteristics of Surface Water
538 and Groundwater in Coastal Watershed, Mekong Delta, Vietnam. The 4th International Conference on
539 Sustainable Future for Human Security, SustaiN 2013. Procedia Environmental Sciences. 20:712-721.
540 Andersen, M.S., Jakobsen, V.N.R., Postma, D. 2005. Geochemical processes and solute transport at the
541 seawater/freshwater interface of a sandy aquifer. Geochimica et Cosmochimica Acta. 69(16):
542 3979-3994.
543 Appelo C.A.J., 1994. Cation and proton exchange, pH variations, and carbonate reactions in a freshening
544 aquifer. Water Resour. Res., 30, 2793-2805.
545 Appelo C.A.J., Postma D., 2005. Geochemistry, Groundwater and Pollution, second edition. Taylor &
546 Francis Group.
547 Bao J., 2005. Two-dimensional numerical modeling of seawater intrusion in Qinhuangdao Region. Master's
548 Thesis. Tongji University, Shanghai, China. (Chinese with English abstract)
549 Barbecot F., Marlin C., Gibert E., Dever L., 2000. Hydrochemical and isotopic characterisation of the
550 Bathonian and Bajocian coastal aquifer of the Caen area (northern France). Applied Geochemistry.
551 15:791-805.
552 Bobba A.G., 2002. Numerical modelling of salt-water intrusion due to human activities and sea-level
553 change in the Godavari Delta, India. Hydrological Sciences. 47(S), S67-S80.
554 Bouchaou L., Michelot J.L., Vengosh A., Hsissou Y., Qurtobi M., Gaye C.B., Bullen T.D., Zuppi G.M.,
555 2008. Application of multiple isotopic and geochemical tracers for investigation of recharge,
556 salinization, and residence time of water in the Souss–Massa aquifer, southwest of Morocco. Journal
557 of Hydrology. 352: 267-287.
558 Cary L., Petelet-Giraud E., Bertrand G., Kloppmann W., Aquilina L., Martins V., Hirata R., Montenegro S.,
559 Pauwels H., Chatton E., Franzen M., Aurouet A., the Team. 2015. Origins and processes of
560 groundwater salinization in the urban coastal aquifers of Recife (Pernambuco, Brazil): A multi-isotope
561 approach. Science of the Total Environment. 530-531:411-429.
562 Chen M., Ma F., 2002. Groundwater resources and the environment in China. Seismological Press. Beijing.
563 pp255-281. (in Chinese)
564 Craig, H., 1961. Standard for reporting concentration of deuterium and oxygen-18 in natural water. Science
565 133, 1833-1834.
566 Creel L., 2003. Ripple effects: Population and coastal regions. Population Reference Bureau. pp1-7.<
567 http://www.prb.org/Publications/Reports/2003/RippleEffectsPopulationandCoastalRegions.aspx>
568 Currell M.J., Cartwright, I., Bradley, D.C., Han, D.M., 2010. Recharge history and controls on groundwater
569 quality in the Yuncheng Basin, north China. Journal of Hydrology. 385: 216-229.
570 Currell M.J., Dahlhaus P.D., Ii H. 2015. Stable isotopes as indicators of water and salinity sources in a
571 southeast Australian coastal wetland: identifying relict marine water, and implications for future
572 change. Hydrogeology Journal. 23: 235-248.
573 Currell M.J., Han D. 2017. The Global Drain: Why China's water pollution problems should matter to the
574 rest of the world. Environment: Science and Policy for Sustainable Development. 59(1): 16-29.
575 de Montety V., Radakovitch O., Vallet-Coulomb C., Blavoux B., Hermitte D., Valles V., 2008. Origin of
576 groundwater salinity and hydrogeochemical processes in a confined coastal aquifer: Case of the Rhône

577      delta (Southern France). Applied Geochemistry. 23: 2337-2349.

578    Edmunds W. M., 1996. Bromine geochemistry of British groundwaters. Mineral. Mag., 60, 275–284.

579    El Yaouti F., El Mandour A., Khattach D., Benavente J., Kaufmann O., 2009. Salinization processes in the
580      unconfined aquifer of Bou-Areg (NE Morocco): A geostatistical, geochemical, and tomographic study.
581      Applied Geochemistry. 24:16-31.

582    Ferguson G., Gleeson T., 2012. Vulnerability of coastal aquifers to groundwater use and climate change.
583      Nature Climate Change. 2, 342-345.

584    Fidelibus M.D., Giménez E., Morell I., Tulipano L., 1993. Salinization processes in the Castellon Plain
585      aquifer (Spain). In: Custodio, E., Galofré, A. (Eds.), Study and Modelling of Saltwater Intrusion into
586      Aquifers. Centro Internacional de Métodos Numéricos en Ingeniería, Barcelona, pp267-283.

587    Garing C., Luquot L., Pezard P.A., Gouze P., 2013. Geochemical investigations of saltwater intrusion into
588      the coastal carbonate aquifer of Mallorca, Spain. Applied Geochemistry. 39:1-10.

589    Ghassemi F., Chen T.H., Jakeman A.J., Jacobson G., 1993. Two and three-dimensional simulation of
590      seawater intrusion: performances of the "SUTRA" and "HST3D" models. AGSO J.
591      Aust.Geol.Geophys. 14(2-3):219-226.

592    Ghiglieri G., Carletti A., Pittalis D., 2012. Analysis of salinization processes in the coastal carbonate aquifer
593      of Porto Torres (NW Sardinia, Italy). Journal of Hydrology. 432-433:43-51.

594    Giambastiani B.M.S., Antonellini M., Oude Essink G.H.P., Stuurman R.J., 2007. Saltwater intrusion in the
595      unconfined coastal aquifer of Ravenna (Italy): A numerical model. Journal of Hydrology. 340:91-104.

596    Giménez-Forcada E., 2010. Dynamic of sea water interface using hydrochemical facies evolution diagram,
597      Ground Water. 48, 212-216.

598    Gingerich S., Voss C., 2002. Three-dimensional variable-density flow simulation of a coastal aquifer in
599      southern Oahu, Hawaii, USA, in Proceedings SWIM17 Delft 2002, edited by R. Boekelman,
600      pp.93-103, Delft Univ. of Technol., Delft, Netherlands.

601    Han D.M., Kohfahl C., Song X.F., Xiao G.Q., Yang J.L., 2011. Geochemical and isotopic evidence for
602      palaeo-seawater intrusion into the south coast aquifer of Laizhou Bay, China. Applied Geochemistry,
603      26(5):863-883.

604    Han D.M., Song, X.F., Currell, M.J., Yang, J.L., Xiao G.Q. 2014. Chemical and isotopic constraints on the
605      evolution of groundwater salinization in the coastal plain aquifer of Laizhou Bay, China. Journal of
606      Hydrology 508: 12-27.

607    Han D., Post V.E.A., Song X., 2015. Groundwater salinization processes and reversibility of seawater
608      intrusion in coastal carbonate aquifers. Journal of Hydrology. 531:1067-1080.

609    Han, D., Song, X., Currell, M. 2016a. Identification of anthropogenic and natural inputs of sulfate into a
610      karstic coastal groundwater system in northeast China: evidence from major ions, $\delta^{13}C_{DIC}$ and $\delta^{34}S_{SO4}$.
611      Hydrology and Earth System Sciences 20(5): 1983-1999.

612    Han, D., Currell, M.J., Cao, G. 2016b. Deep challenges for China's war on water pollution. Environmental
613      Pollution. 218: 1222-1233.

614    Han Z., 1988. Seawater intrusion into coastal porous aquifer- a case study of the alluvial plain of Yang
615      River and Dai River in Qinhuangdao City. China University of Geosciences, Beijing, China. (Chinese
616      with English abstract)

617    Han Z., 1990. Controlling and harnessing of the seawater intrusion the alluvial plain of Yang River and Dai
618      River in Qinhuangdao.Geoscience (Journal of Graduate School, China University of Geosciences).
619      4(2):140-151. (Chinese with English abstract)

620    Hebei Geology Survey, 1987. Report of regional geological and tetonic background in Hebei Province.

621       Internal materials.

622 Hui G., 2009. Characteristics and formation mechanism of hydrochemistry of geothermal water in Danihe,
623       Funing District of Qinhuangdao region. Science & Technology Informaion. 9:762-763. (in Chinese)

624 IAEA/WMO, 2006. Global Network of Isotopes in Precipitation. The GNIP Database, Vienna.
625       <http://www-naweb.iaea.org/napc/ih/IHS_resources_gnip.html>.

626 IPCC, Climate Change 2007: The Physical Science Basis, Contribution of Working Group I to the Fourth
627       Assessment Report of the Intergovernmental Panel on Climate Change, S. Solomon et al., Eds.
628       (Cambridge Univ. Press, Cambridge, 2007).

629 Jones B.F., Vengosh A., Rosenthal E. Yechieli Y., 1999. Geochemical investigations. In: Bear et al. (eds)
630       Seawater Intrusion in Coastal Aquifers - Concepts, Methods and Practices, pp51-72.

631 Langevin C.D., Zygnerski M.R., White J.T., Hughes J.D., 2010. Effect of sea-level rise on future coastal
632       groundwater resources in southern Florida, USA. SWIM21-21st Salt Water Intrusion Meeting. Azores,
633       Portugal., June 21-26, 2010. Pp125-128.

634 Larsen, F., Tran, L.V., Hoang, H.V., Tran, L.T., Chistiansen, A.V., Pham, N.Q., 2017. Groundwater salinity
635       influenced by Holocene seawater trapped in the incised valleys in the Red River delta plain. Nature
636       Geoscience 10: 376-382.

637 Lee, S., Currell, M., Cendon, D.I., 2016. Marine water from mid-Holocene sea level highstand trapped in a
638       coastal aquifer: Evidence from groundwater isotopes, and environmental significance. Science of the
639       Total Environment. 544: 995-1007

640 Masterson J.P., 2004. Simulated interaction between freshwater and saltwater and effects of ground-water
641       pumping and sea-level change, Lower Cape Cod aquifer system, Massachusetts: U.S. Geological
642       Survey Scientific Investigations Report 2004-5014, 72 p.

643 Mazi, K., Koussis, A.D., Destouni, G., 2014. Intensively exploited Mediterranean aquifers: proximity to
644       tipping points and control criteria for sea intrusion. Hydrol. Earth Syst. Sci. 18, 1663-1677.

645 Meng F., 2004. Rational development of groundwater resources on the coastal zone of Qinhuangdao area.
646       Marine Geology Letters. 20(12):22-25. (Chinese with English abstract)

647 Michael H.A., Post V.E.A., Wilson A.M., Werner A.D. 2017. Science, society and the coastal groundwater
648       squeeze. Water Resources Research. 53. 2610-2617.

649 Mondal N.C., Singh V.P., Singh V.S., Saxena V.K., 2010. Determining the interaction between groundwater
650       and saline water through groundwater major ions chemistry. Journal of Hydrology. 388:100-111.

651 Montenegro S.M.G., de A. Montenegro A.A., Cabral J.J.S.P., Cavalcanti G., 2006. Intensive exploitation
652       and groundwater salinity in Recife coastal plain (Brazil): monitoring and management perspectives.
653       Proceedings 1st SWIM-SWICA Joint Saltwater Intrusion Conference, Cagliari-Chia Laguna, Italy -
654       September 24-29, 2006. pp79-85.

655 Moore W.S., 1996. Large groundwater inputs to coastal waters revealed by 226Ra enrichments. Nature
656       380,612-214.

657 Narayan K.A., Schleeberger C., Bristow K.L., 2007. Modelling seawater intrusion in the Burdekin Delta
658       Irrigation Area, North Queensland, Australia. Agricultural Water Management. 89:217-228.

659 Pan G., Yang Y., Zhang L., 1990. Survey report of geothermal water in Qinhuangdao city of Hebei Province.
660       Team of mineral hydrological and engineering geology from the Bureau of Geology and mineral
661       Resources of Hebei Province, China. (in Chinese)

662 Post V.E.A., 2005. Fresh and saline groundwater interaction in coastal aquifers: Is our technology ready for
663       the problems ahead? Hydrogeology Journal. 13:120-123.

664 Price R.M., Herman J.S., 1991. Geochemical investigation of salt-water intrusion into a coastal carbonate

665    aquifer: Mallorca, Spain. Geological Society of America Bulletin. 103:1270-1279.

666    Pulido-Leboeuf P., 2004. Seawater intrusion and associated processes in a small coastal complex aquifer

667    (Castell de Ferro, Spain). Applied Geochemistry. 19:1517-1527.

668    Radhakrishna I., 2001. Saline fresh water interface structure in Mahanadi delta region, Orissa, India.

669    Environmental Geology. 40(3):369-380.

670    Rahmawati N., Vuillaume J., Purnama I.L.S., 2013. Salt intrusion in Coastal and Lowland areas of

671    Semarang City. Journal of Hydrology. 494:146-159.

672    Robinson M.A., Gallagher D.L., Reay W.G., 1998. Field observations of tidal and seasonal variations in

673    ground water discharge to estuarine surface waters. Ground Water Monitoring and Remediation. 18

674    (1): 83-92.

675    Shen Z., Zhu Y., Zhong Z., 1993. Theoretical basis of hydrogeochemistry. Geological Publishing House.

676    Beijing, China. (in Chinese)

677    Sherif M.M., Singh V.P., 1999. Effect of climate change on sea water intrusion in coastal aquifers.

678    Hydrological Processes 13, 8:1277-1287.

679    Shi M.Q., 2012. Spatial distribution of population in the low elevation coastal zone and assessment on

680    vulnerability of natural disaster in the coastal area of China. Master thesis of Shanghai Normal

681    University, 24–32.(Chinese with English abstract)

682    Simpson, M.J., Clement, T.P., 2004. Improving the worthiness of the Henry problem as a benchmark for

683    density-dependent groundwater flow models. Water Resources Research 40 (1), W01504

684    doi:10.1029/2003WR002199.

685    Sivan O., Yechieli Y., Herut B., Lazar B., 2005. Geochemical evolution and timescale of seawater intrusion

686    into the coastal aquifer of Israel. Geochimica et Cosmochimica Acta. 69(3):579-592.

687    Smith A.J., Turner J.V., 2001. Density-dependent surface water-groundwater interaction and nutrient

688    discharge in the Swan-Canning Estuary. Hydrolological Processes. 15:2595-2616.

689    SOA (State Oceanic Administration of the People's Republic of China), 2015. China's Marine Environment

690    Bulletin: 2014. Released 11th March, (in Chinese).

691    Sun J., Yang Y., 2007. Seawater intrusion characteristics in Qinhuangdao. Journal of Environmental

692    Management College of China. 17(2):51-54. (Chinese with English abstract)

693    UN Atlas, 2010. UN Atlas: 44 Percent of us Live in Coastal Areas.

694    <http://coastalchallenges.com/2010/01/31/un-atlas-60-of-us-live-in-the-coastal-areas/>.

695    Vengosh A., Spivack A.J., Artzi Y., Ayalon A. 1999. Geochemical and boron, strontium, and oxygen

696    isotopic constraints on the origin of the salinity in groundwater from the Mediterranean coast of Isreal.

697    Water Resources Research. 35(6): 1877-1894.

698    Walraevens, K., Cardenal-Escarcena, J., Van Camp, M., 2007. Reaction transport modelling of a freshening

699    aquifer (Tertiary Ledo-Paniselian Aquifer, Flanders-Belgium). Applied Geochemistry. 22: 289-305.

700    Wang, J., Yao, P., Bianchi, T.S., Li, D., Zhao, B., Cui, X., Pan, H., Zhang, T., Yu, Z., 2015. The effect of

701    particle density on the sources, distribution, and degradation of sedimentary organic carbon in the

702    Changjiang Estuary and adjacent shelf. Chemical Geology. 402:52-67.

703    Weber, K., Stewart, M., 2004. A critical analysis of the cumulative rainfall departure concept. Ground

704    Water 42 (6), 935–938.

705    Werner, A.D., 2010. A review of seawater intrusion and its management in Australia. Hydrogeology Journal.

706    18(1):281-285.

707    Werner A.D., Bakker M., Post V.E.A., Vandenbohede A., Lu C., Ataie-Ashtiani B., Simmons C.T., Barry

708    D.A., 2013. Seawater intrusion processes, investigation and management: Recent advances and future

709    challenges. Advances in Water Resources.51:3-26.

710    Werner A.D., Simmons C.T., 2009. Impact of sea-level rise on seawater intrusion in coastal aquifers.
711        Ground Water. 47:197-204.

712    Westbrook S.J., Rayner J.L., Davis G.B., Clement T.P., Bjerg P.L., Fisher S.J., 2005. Interaction between
713        shallow groundwater, saline surface water and contaminant discharge at a seasonally and tidally forced
714        estuarine boundary. Journal of Hydrology, 302:255-269.

715    Wilhite D.A., 1993.Drought Assessment, Management, and Planning: Theory and Case Studies. Springer U
716        S. p628.

717    Xu G., 1986. Analysis of seawater intruding into aquifer system in Beidaihe Region.Hydrogeology &
718        Engineering Geology. 2:7-10. (in Chinese)

719    Xue Y.Q., Wu J.C., Ye S.J., Zhang Y.X., 2000. Hydrogeological and hydrogeochemical studies for salt
720        water intrusion on the South Coast of Laizhou Bay, China. Ground Water. 38, 38-45.

721    Yang L., 2011. Formation mechanism of bedrock fracture type-geothermal water in Qinhuangdao area.
722        West-china Exploration Engineering. Urumchi, China. 10:151-152. (in Chinese)

723    Yang Y., Gao S., Xie Y., 2008. Assessment and control countermeasures of seawater intrusion hazard on
724        Qinhuangdao Region. The Chinese Journal of Geological Hazard and Control. 19(3):139-143.
725        (Chinese with English abstract)

726    Yang Y., He Q., Xie Y., Cao C., 1994. Grey model prediction of seawater intrusion of Qinhuangdao. The
727        Chinese Journal of Geological Hazard and Control. 5(sup.):181-183. (Chinese with English abstract)

728    Yechieli Y., Kafri U., Sivan O., 2009. The inter-relationship between coastal sub-aquifers and the
729        Mediterranean Sea, deduced from radioactive isotopes analysis. Hydrogeology Journal. 17:265-274.

730    Zang W., Liu W., Guo J., Zhang X., 2010. Geological hazards of seawater intrusion and its control
731        measures in Qinhuangdao City, Hebei Province. The Chinese Journal of Geological Hazard and
732        Control. 21(4):120-125. (Chinese with English abstract)

733    Zeng J., 1991. Geochemistry of geothermal water in Qinhuangdao area, Hebei Province. Bull. Institute of
734        Hydrogeology and Engineering Geology, Chinese Academy of Geological Sciences. 7:111-127.

735    Zhang B., 2012. Mechanism of Seawater Intrusion Using Hydrochemistry and Environmental Isotopes in
736        Qinhuangdao Yang Dai River Plain. Master's Thesis. Xiamen University, Fujian, China. (Chinese with
737        English abstract)

738    Zhang Q., Volker R.E., Lockington D.A., 2004. Numerical investigation of seawater intrusion at
739        Gooburrum, Bundaberg, Queensland, Australia. Hydrogeol. J. 12 (6), 674-687.

740    Zuo W., 2006. Survey and Research on Seawater Intrusion in the Yandaihe Plain of Qinhuangdao City.
741        Doctoral Thesis. China University of Geosciences, Beijing, China. (Chinese with English abstract)

742    Zuo W., Yang Y., Dong Y., Liang M., 2009. The numerical study for seawater intrusion in Yanghe and
743        Daihe coastal plain of Qinhuangdao City. Journal of Natural Resources. 24(12):2087-2095. (Chinese
744        with English abstract)

745

746

747

748

749

750

751

752
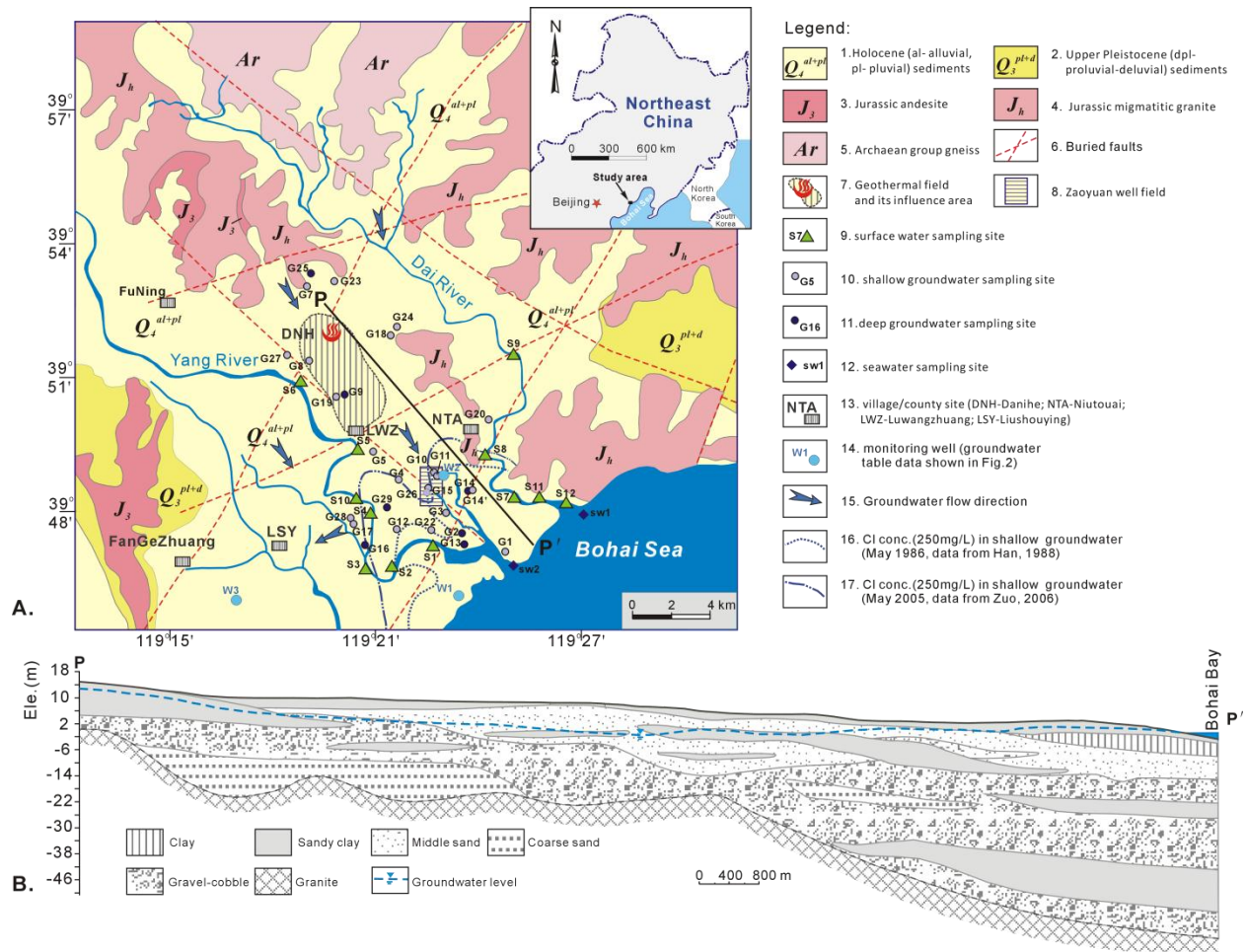
Figure 1. Location map (A.) for showing geological background and water sampling sites in the study area, and (B.) hydrogeological cross-section of Yang-Dai River Plain (P-P′ in A.) (modified from Han, 1988). The surface area covered from >250 mg Cl/L contour line to coastline refers the seawater zones.
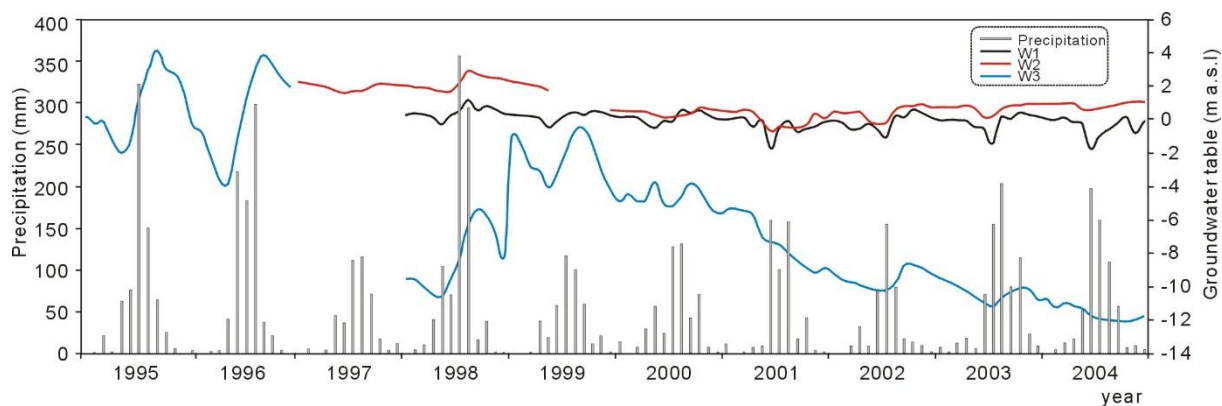
Figure 2. Distribution of precipitation and dynamics of water table in the study area. Locations of the monitoring wells (W1, W2 and W3) can be seen from Fig. 1.
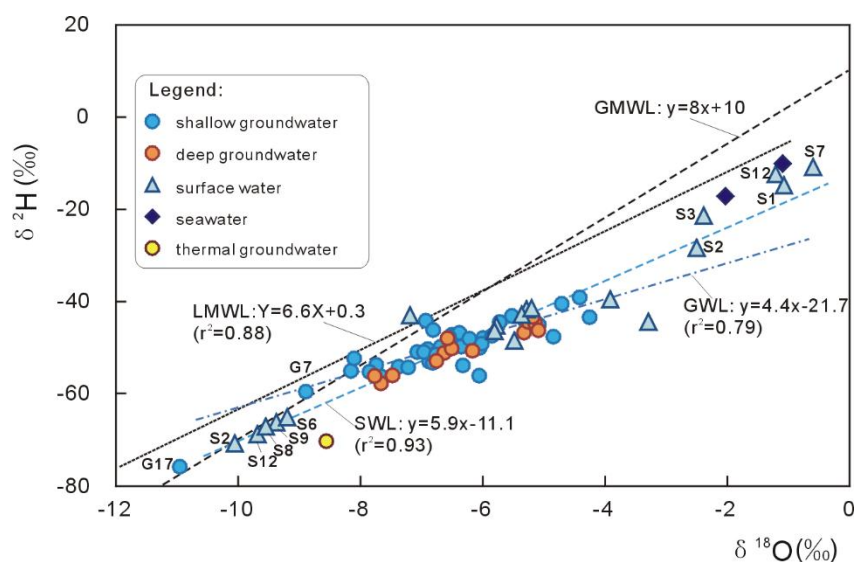
Figure 3. Stable isotope compositions of different water samples collected from the study area
LMWL - local meteoric water line; GMWL – global meteoric water line (Craig, 1961); GWL – groundwater line; SWL – surface (river) water line.
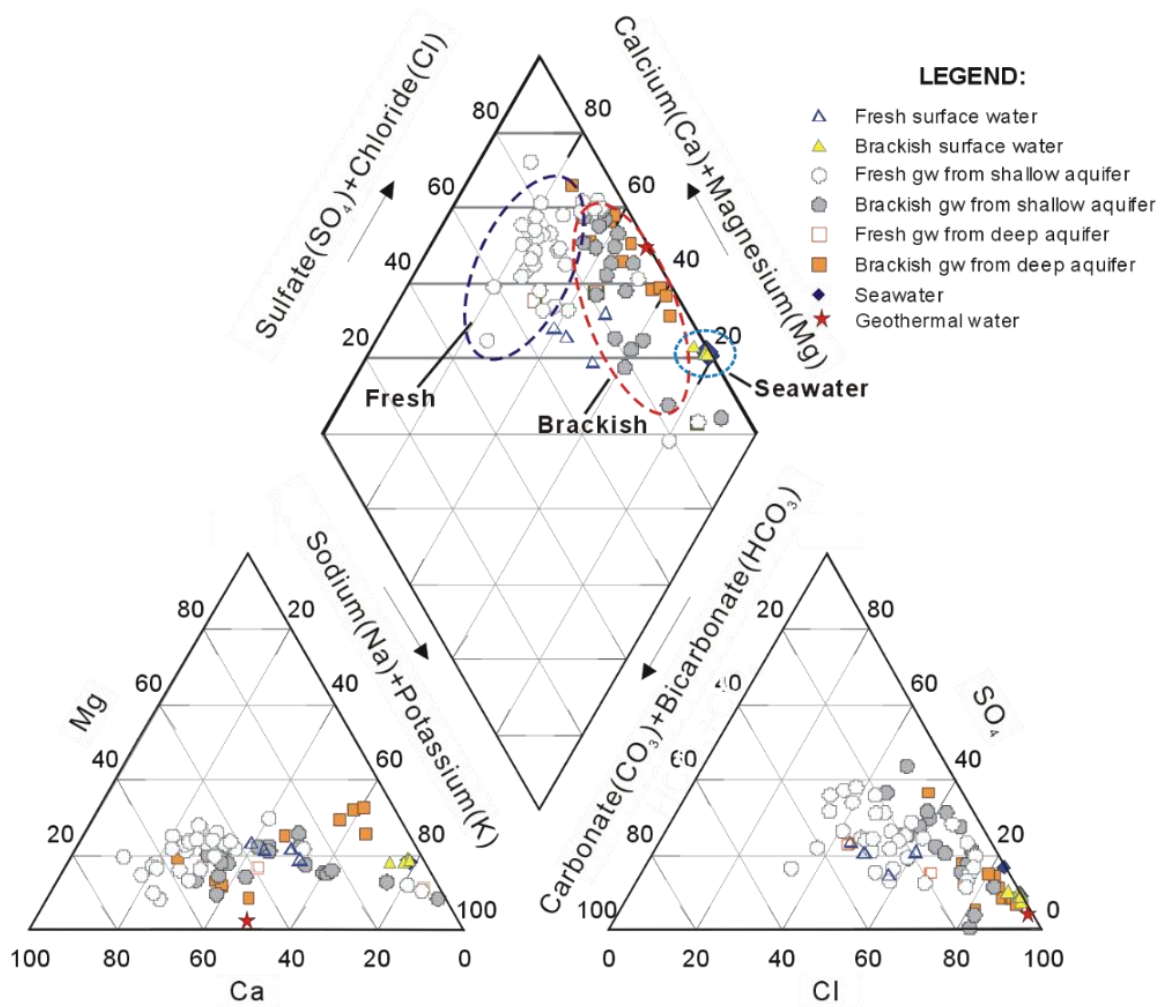
Figure 4. Piper plot of different water samples
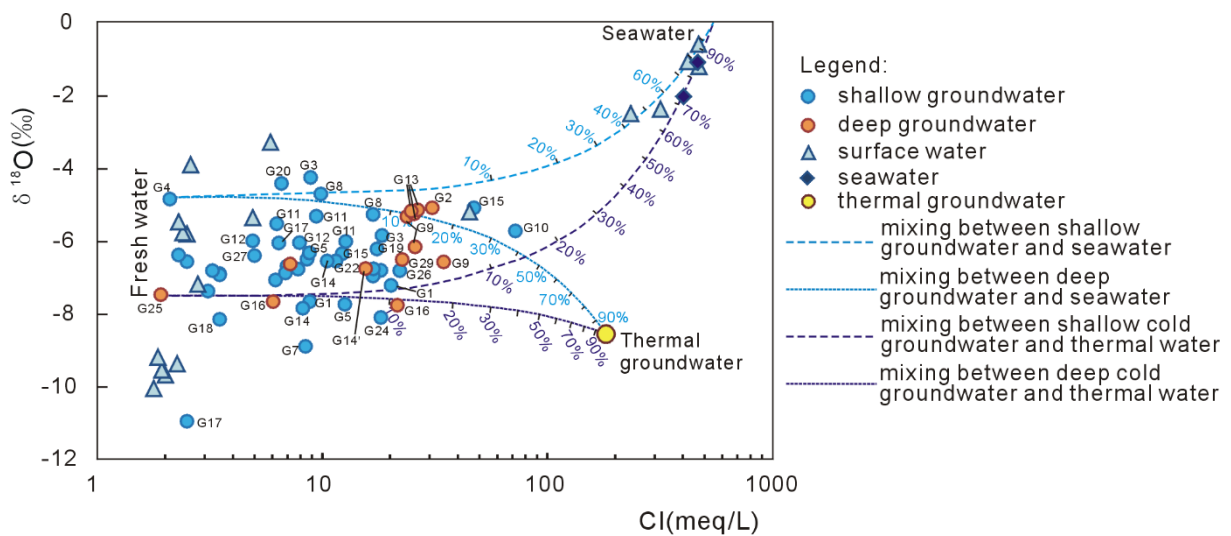
Figure 5. Relationship between chloride content and isotopic signature of different water samples as a means to differentiate mixing processes in the area. The data of thermal water are from Zeng (1991).

783

784
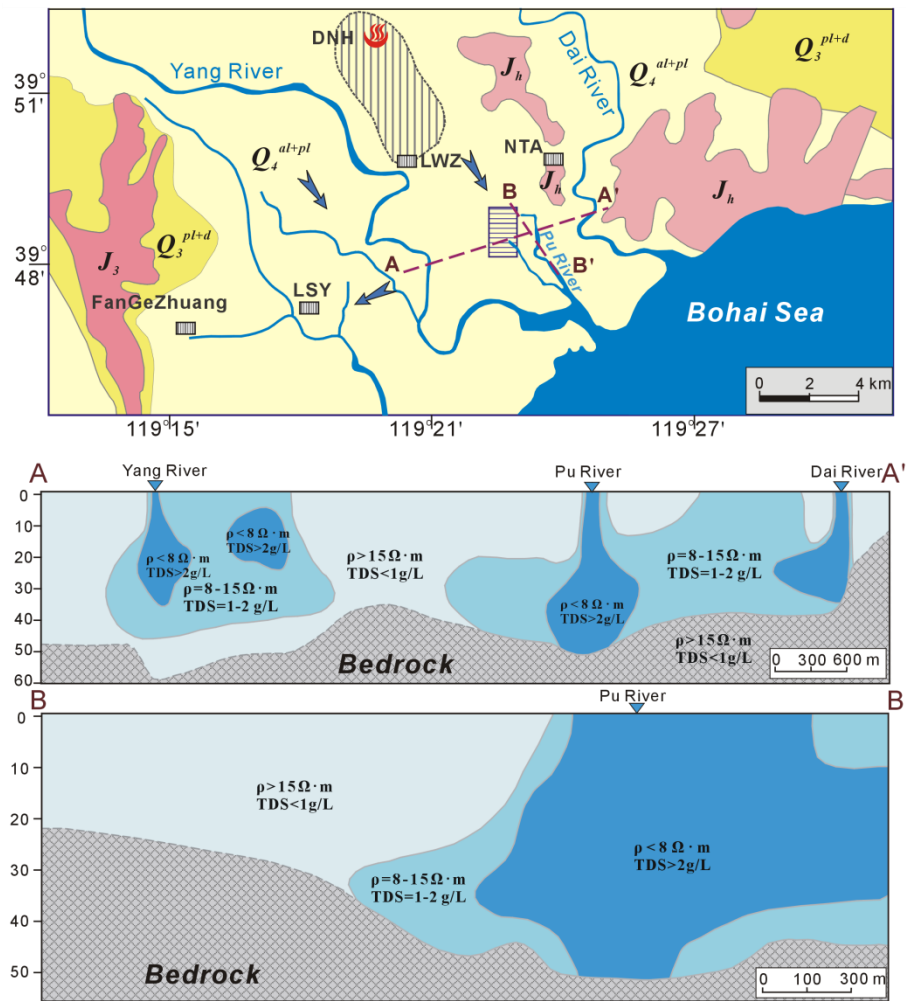
785 Figure 6. Cross-sections showing results obtained from application of geophysical resistivity method
786 (employed in May, 2004, data and methods described in Zuo, 2006)

787

788

789     (a)                                    (b)

790
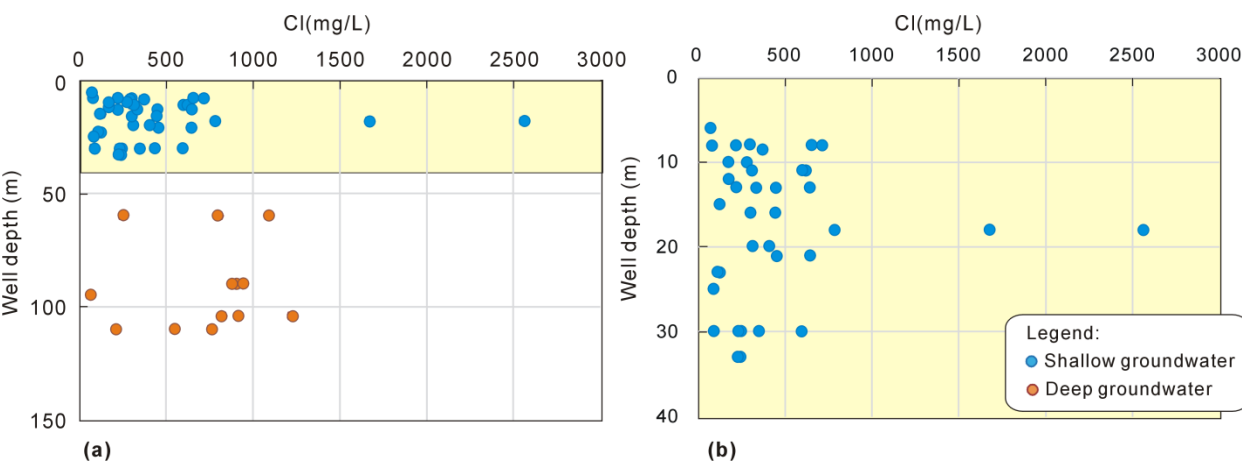
791 Figure 7. Chloride concentration vs. well depth for groundwater samples.

792
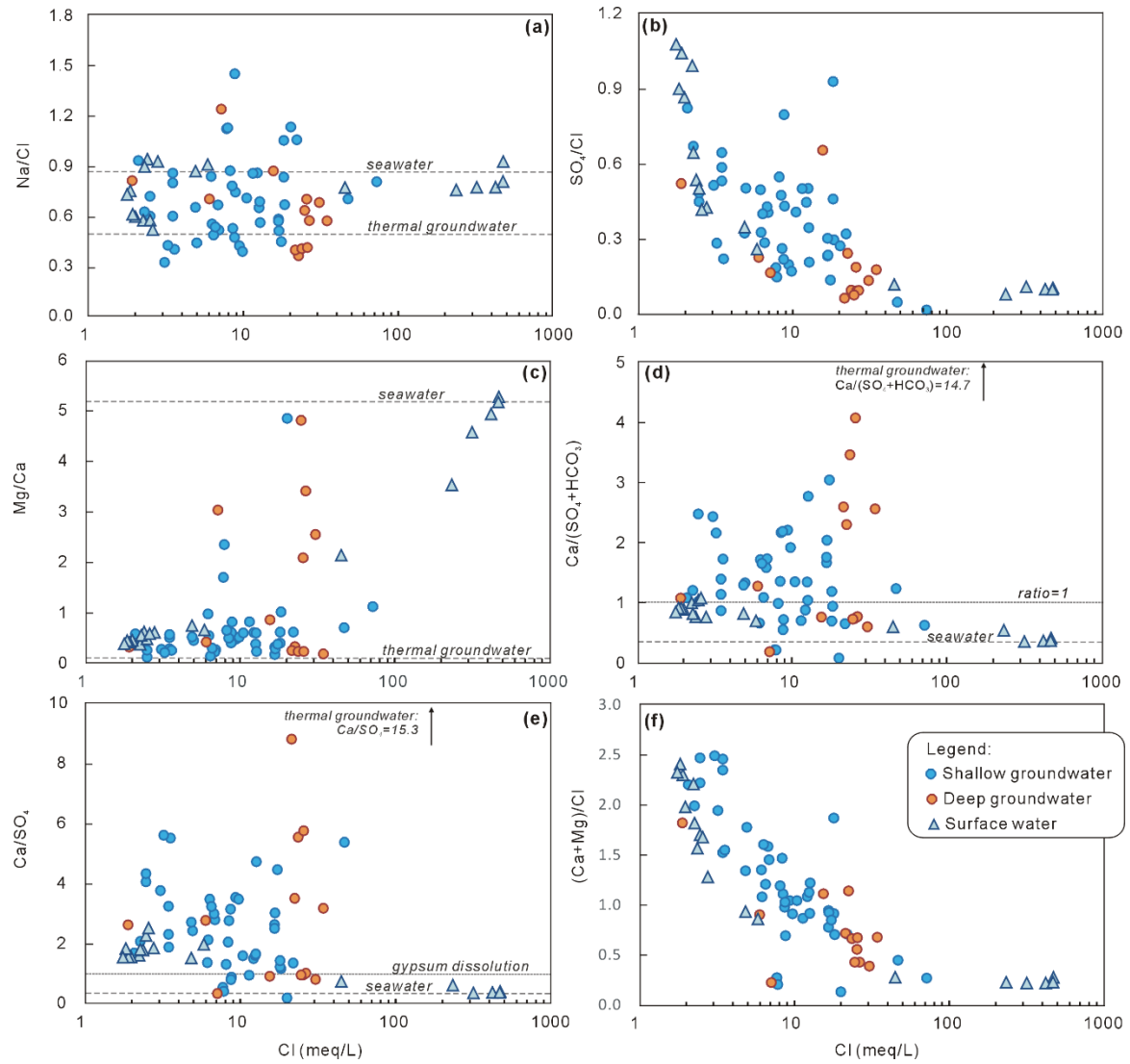
Figure 8. Molar ratios of major ions versus chloride concentrations for different water samples from the study area

812

813
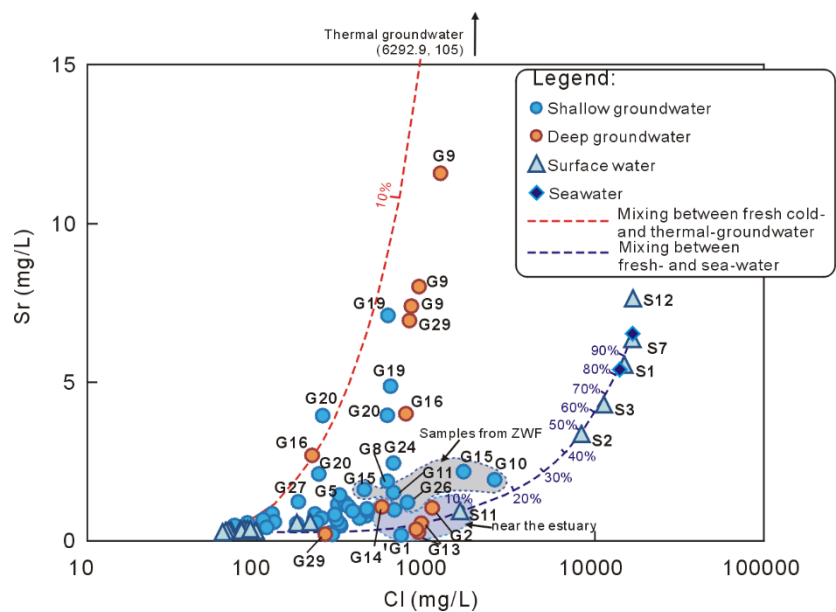
816  Figure 9. Chloride versus strontium concentrations of different water samples ZWF- Zaoyuan well field

817
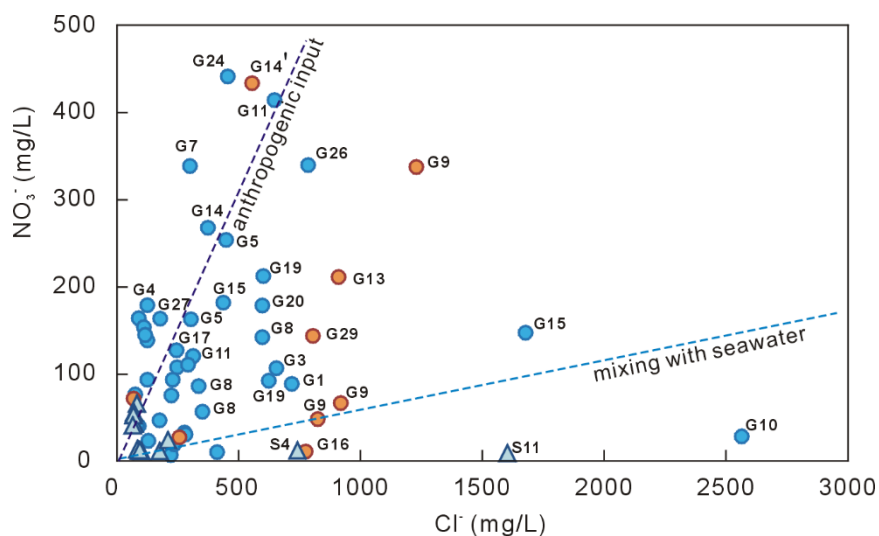
819  Figure 10. Plot of chloride versus nitrate concentrations in groundwater, with seawater and anthropogenic
820  pollution mixing trajectories

821

822
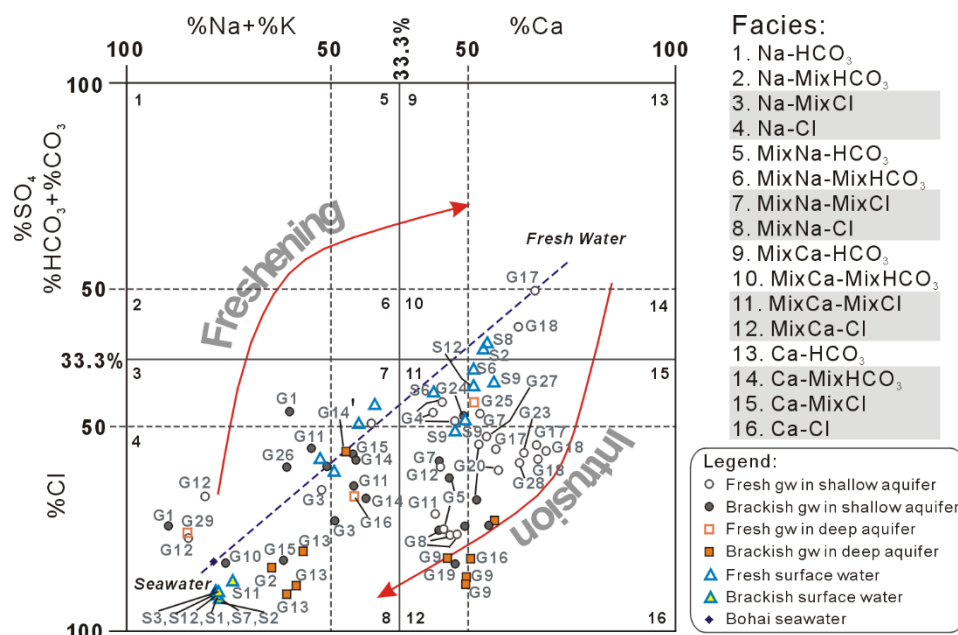
Figure 11. Hydrogeochemical facies evolution diagram (HFE-D) for the collected water samples
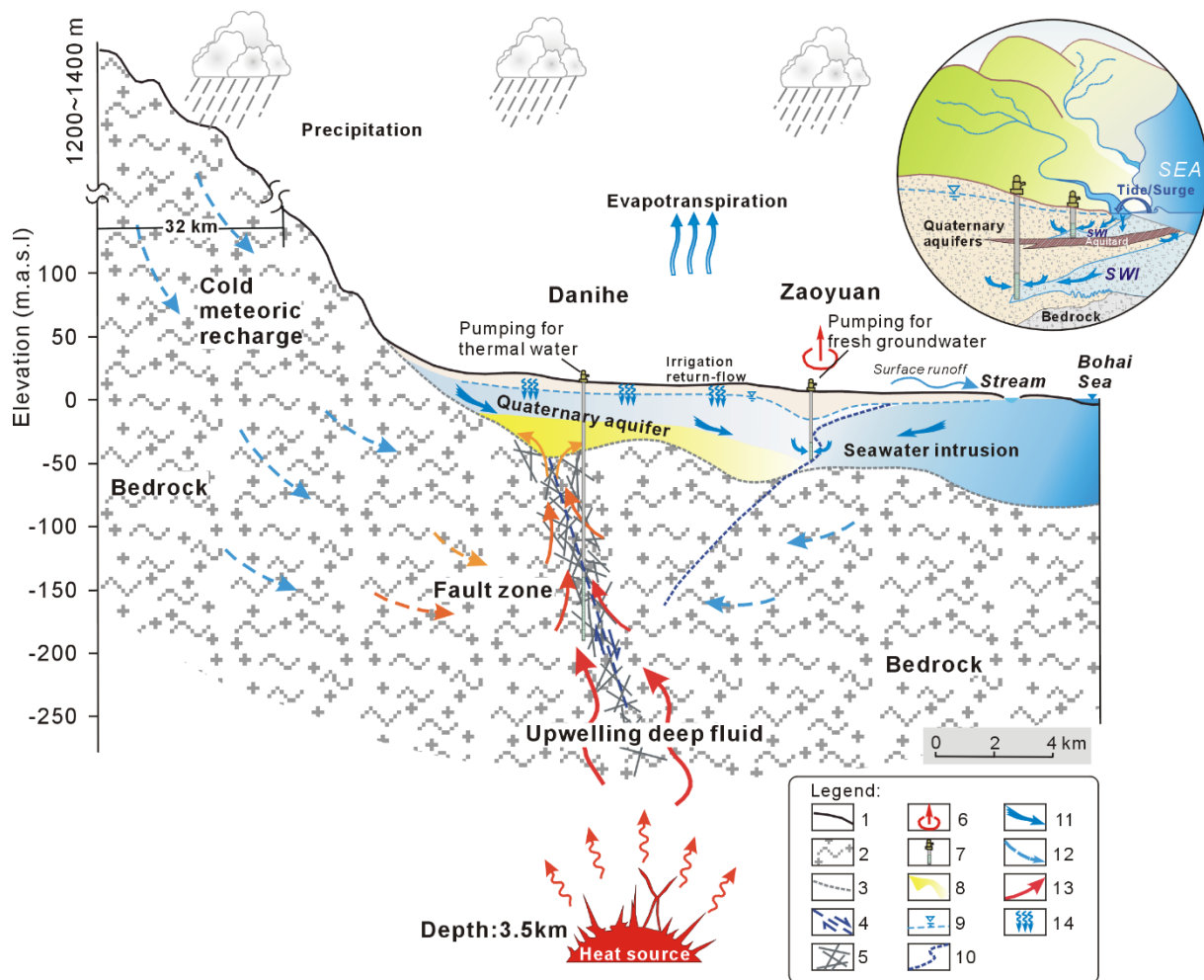
834
835 Figure 12. Conceptual model of groundwater flow system in the Yang-Dai River coastal plain
836 Explanation: 1- Land surface; 2- Bedrock; 3- Boundary between Quaternary sediments and bedrock;
837 4-Fault; 5- Permeable fracture zone; 6- Concentrated groundwater pumping zone; 7- Pumping wells; 8-
838 Zone affected by upflow of geothermal fluids; 9- Water table; 10- Potential interface between fresh- and
839 salt-water; 11-Groundwater flow direction in Quaternary aquifers; 12- Groundwater flow in bedrocks; 13-
840 Geothermal groundwater flow direction; 14- Irrigation return-flow.
841
842
843
844
845
846
847